CEAS Space Journal
https://doi.org/10.1007/s12567-025-00649-0

ORIGINAL PAPER

Experimental investigations of fluid-to-vehicle interactions during a reusable launcher's touchdown impact

Caroline Krämer[1] · **Lars Witte**[1]

Received: 26 August 2024 / Revised: 21 May 2025 / Accepted: 15 July 2025

Abstract
Several programmes are dedicated worldwide to the development of reusable vertical take-off vertical landing (VTVL) launch vehicles. Thereby, the touchdown event with its associated impact forces and shocks poses load cases to the vehicle being new in the launcher domain. Furthermore, the application of related knowledge from planetary, exploration-type landers has to be taken cautiously due to the differences between those types of vehicle, particularly with regard to their tank configuration and structural sizing. Depending on flight test conditions and operational concept, non-neglectable amounts of liquid propellant can still be inside the tanks at landing and interact with the vehicle. These interactions cause dynamic and structural effects that affect the landing stability and structural integrity of the vehicle. This study aims to experimentally investigate the fluid–vehicle interactions of a fully functional touchdown demonstrator during touchdown. For this, a vehicle landing engineering model is equipped with a circular cylindrical tank and a series of touchdown tests with varying horizontal landing velocities and fill levels is conducted. Thereby, the main objectives are to prove repeatable landing behaviour under sloshing impact for constant landing conditions, to characterise the fluid impact on landing stability and to investigate the fluid–structure interactions on the tank. Therefore, test data of different test cases are compared and analysed with regard to dynamic behaviour and structural responses.

Keywords Propellant sloshing · VTVL · Landing stability · Fluid–vehicle interaction

1 Introduction

An increasing number of space flying nations and the rise of private space flight renewed the idea of reusability as an enabler for decreasing launch costs and increasing launch flexibility. Several programmes have been established worldwide with the common goal to accelerate the development of reusable space launch vehicles. In Europe, ESA is funding the Themis programme. In cooperation with the Horizon Europe project SALTO, Themis aims to develop the first European reusable rocket prototype [1]. Within SALTO the landing phase of the vertical take-off vertical landing (VTVL) vehicle Themis will be tested and validated. Fly/entry/re-fly cycles will be flown [2]. One of the most critical phases of these cycles is the event of touchdown, since an unsuccessful landing will cause the loss of the vehicle.

As reusable spacecraft rely on re-ignitable engines for deceleration and attitude control, their tanks are partly filled with remaining liquid propellant during touchdown. The free surface within a partly filled tank allows the fluid to perform a sloshing movement when excited. Depending on the amount of sloshing fluid, this has an impact on the vehicle dynamics. As for conventional lunar and planetary landers, the amount of remaining propellant at the moment of touchdown is comparably small, the sloshing effects during touchdown are in most cases neglectable [3]. For reusable space flight, VTVL vehicles are under development, for which significantly larger amounts of propellant are present at the moment of touchdown. This can be due to ballistic extra masses required for test flights, or due to extra propellant needed for take-off from another celestial body, as in SpaceX' Lunar Starship when re-ascending from the moon. The combination of larger propellant mass to total mass ratio and the higher height of centre of gravity (h_{COG}) to footpad diameter (D_F) ratio, typical for VTVL vehicles, makes them more prone to fluid–vehicle interactions. These can be divided into dynamic effects that affect the landing stability

✉ Caroline Krämer
caroline.kraemer@dlr.de

[1] German Aerospace Center, Institute of Space Systems, Landing and Exploration Technologies, Bremen, Germany

Published online: 07 August 2025

and the impact behaviour and structural effects, such as fluid–tank interactions, which might induce load cases that affect the general vehicle and tank design. To ensure a stable landing under the impact of sloshing fluid and structural integrity at the moment of touchdown, the investigation of fluid-induced effects is indispensable for the design of reusable VTVL vehicles.

Numerous studies have been conducted to analyse and model inflight fluid sloshing with regard to its impact on spacecraft dynamics, flight stability and guidance, navigation and attitude control systems [4–13]. Several others have been dedicated to sloshing reduction methods for VTVL vehicles [14–16]. The sloshing impact on spacecraft landing dynamics has been investigated numerically and experimentally by Anii et al. and Furuich [17, 18]. However, their work is restricted to sloshing in spherical tanks in small body landers under micro-gravity conditions. Roithmayr and Pei are, to the author's knowledge, the only ones to investigate the effect of propellant sloshing on touchdown stability boundaries for landing space vehicles under lunar gravity [19]. Their work addresses a two-dimensional multibody modelling approach, consisting of a rigid pendulum, representing the sloshing fluid, attached to a rigid lander body. They offer first insights on how different propellant sloshing states before touchdown affect the landing stability for varying landing conditions and provide preliminary design trends. Being intended for the early design phase, no details of landing gear articulation, energy absorption and elasticity are considered. Therefore, the impact of these parameters on the landing dynamics is being neglected and no options for the examination of fluid–structure interactions during touchdown are given. For the detailed design of a reusable VTVL vehicle, further investigations of the sloshing impact are required, which deviate from the rigid modelling approach and thus provide dynamic interactions, structural responses and interface forces for a specific spacecraft. While theoretical and numerical studies can cover the examination of a broad spectrum of test cases and vehicle forms, these models underlie assumptions and approximations and hence rely on experimental data for validation. Therefore, the aim of this paper is the experimental investigation of fluid–lander interaction of a fully functional touchdown demonstrator (TDD) during touchdown. Thereby, the main objectives are

1) to prove repeatable landing behaviour under fluid impact and thus prove that constant landing conditions can be provided and results are comparable for further investigation,
2) the investigation and characterisation of the fluid sloshing impact on dynamical behaviour with regard to landing stability and
3) the analysis of the fluid–structure interaction of the tank with regard to structural responses induced by the fluid under varying landing conditions. The obtained data can later be used to validate numerical models, with which parametric studies can be performed. To serve as a validation model, the TDD must represent all kinematic and dynamic dependencies of a real reusable launch vehicle, but must not be a specific subscale model. For this a lander engineering model is expanded by a circular cylindrical tank and a series of touchdown test with varying horizontal landing velocities and fill levels is conducted. A description of the test setup, including a detailed description of the TDD, is given in Sect. 2. In Sect. 3 test data are analysed, interpreted and discussed with regard to the three before defined main test objectives. A final conclusion is drawn and open questions are formulated in Sect. 4.

2 Test setup

2.1 Touchdown demonstrator

The Touchdown Demonstrator (TDD) design (Fig. 1) is based on the Lander Engineering Model (LEM) design (Fig. 1(1)) [20]. The already existing LEM is adapted to accommodate a fluid containing tank (Fig. 1(3)). As vertically landing vehicles tend to have a higher H_{COG}/D_F ratio

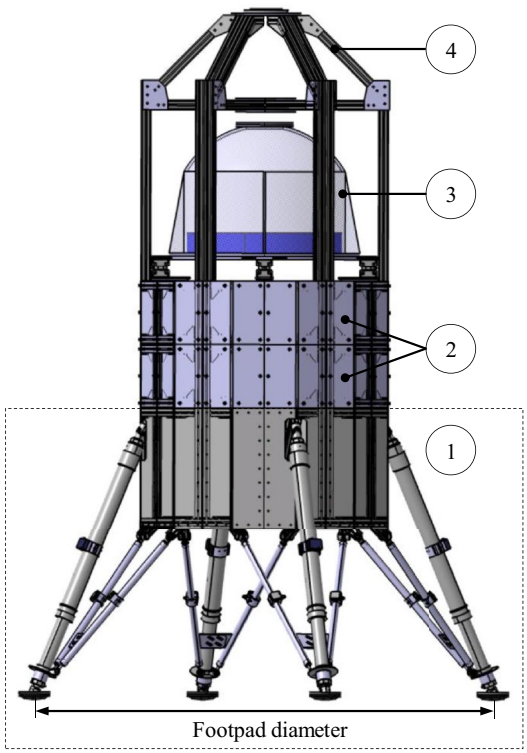

Fig. 1 Touchdown demonstrator, 1: Vehicle aftbay with four landing legs in 'inverted tripod' configuration, 2: Reinforcement Rings, 3: Tank, 4: Robot Adapter and Horizontal Reinforcement

than conventional planetary landers, the tank is to be positioned at the highest possible position as technically permitted by the test facility. The maximum height of the TDD is limited by the working space of the test facility, which is used to lift the TDD to its drop position, and the maximum drop height, resulting from the maximum intended vertical drop velocity, described more in detail in the following sub-chapter. The resulting maximum TDD height is approx. 3000 mm. To ensure torsional stiffness, two reinforcement rings (Fig. 1(2)) are implemented. At the top of the TDD a robot interface (Fig. 1 (4)) is combined with a horizontal reinforcement structure, that prevents the vertical profiles from bending inwards when being lifted by the robot. The maximum total mass of the TDD is 500 kg, corresponding to the maximal static load bearing capacity of the robot. To ensure a constant TDD mass throughout all test cases, with and without fluid, extra masses can be accommodated within the TDD's tip.

The LEM, depicted in Fig. 2, is used in a four-legged inverted tripod configuration, equivalent to state-of-the-art vertically landing vehicles [21, 22]. Every leg consists of one primary telescopic strut (b), including an internal energy absorption mechanism, two secondary struts (a) and a fixed aluminium-rubber footpad. Cardan joints (d) serve as interfaces between the primary struts and the lander body (e). Interfaces (g) at the lander body baseplate (f) provide a connection for the secondary struts.

Leg 1 and adjacent leg 2, which correspond to the front and rear left leg respectively, are being equipped with sensors, as shown in Fig. 3. Triaxial force sensors ($F_{FP,1}$ and $F_{FP,2}$) are placed between the footpad and the primary strut. The sensors are integrated such that the sensors' z-axes are aligned with the primary struts. Uniaxial force sensors ($F_{PS1,LB}$ and $F_{PS2,LB}$) are placed at the top of the primary struts, right before the cardan lander body interface, the sensors' measurement axes aligned with the primary strut axes. Leg 1 is additionally equipped with accelerometers, which are positioned on the footpad (Acc_{FP1}) as well as on all three interfaces to the lander body ($Acc_{PS1,LB}$, $Acc_{SS11,LB}$ and $Acc_{SS12,LB}$). The accelerometers measure the acceleration along the global vertical axis. On the baseplate inside the lander body a triaxial accelerometer (Acc_{LB}) is positioned.

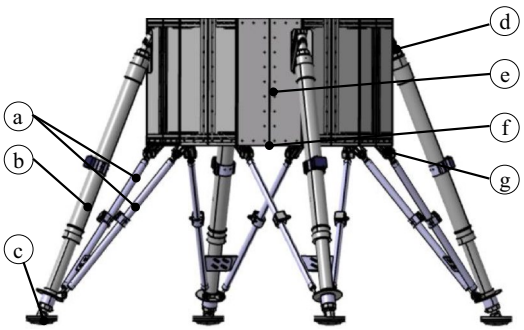

Fig. 2 Lander Engineering Model used as Platform for TDD Design

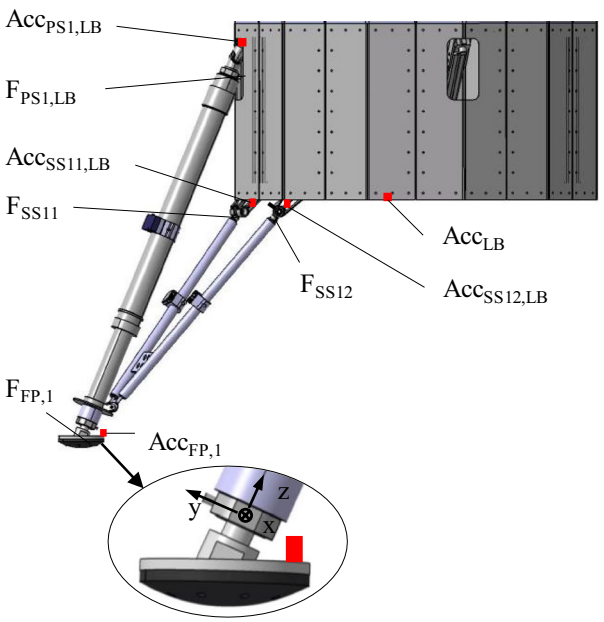

Fig. 3 Sensor locations (leg and body)

The tank is made of transparent acrylic glass to visually detect the fluid movement. De-mineralised water is chosen as test fluid, as its parameters are well known and it poses no handling risks. It is non-toxic and can be coloured for better visual detection. The tank is supported by four triaxial force sensors (F_{T1}–F_{T4}). Additionally, two uniaxial accelerometers are placed on the tank wall (Acc_{Tx+} and Acc_{Tx-}), as shown in Fig. 4. The accelerometers are installed at about 10 cm tank height, which is about the height of the water edge for 50 l of water. Further, a triaxial accelerometer is attached from underneath to the tank bottom plate.

2.2 Test facility

The tests are performed in the Landing and Mobility Test Facility (LAMA) at the DLR-institute of space systems in Bremen [23], shown in Fig. 5. The LAMA laboratory consists of a test cell, surrounded by a protective fence and a control and work space outside the fence. The test cell includes a landing area and is equipped with a 6-axis industrial robot system KR500 with an additional rail track system for horizontal movement (max. 1.5 m/s in both directions). As the robot follows a pre-programmed path, the test sequence can be completely automated and constant drop conditions and a precision landing can be ensured. At the release point the test object will have the predefined horizontal velocity. The release height has to be chosen with respect to the test object's size, so that the required vertical landing

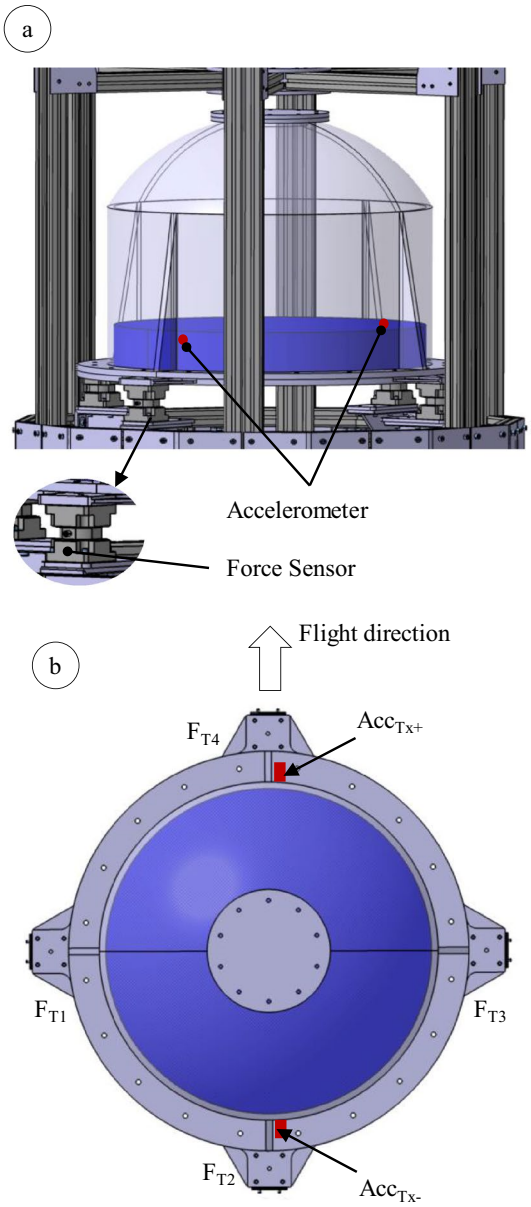

Fig. 4 Sensor locations (tank)

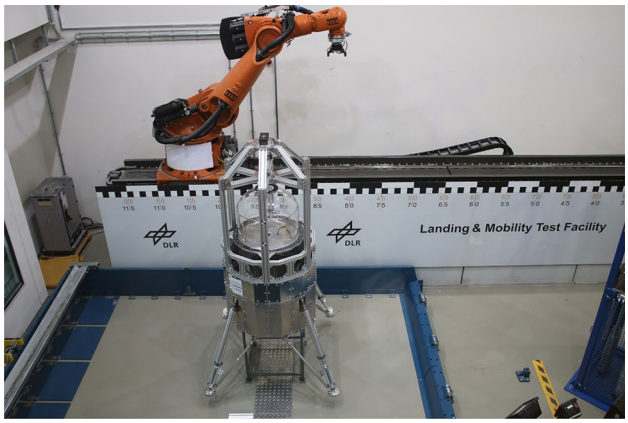

Fig. 5 Landing and mobility test facility at DLR Bremen

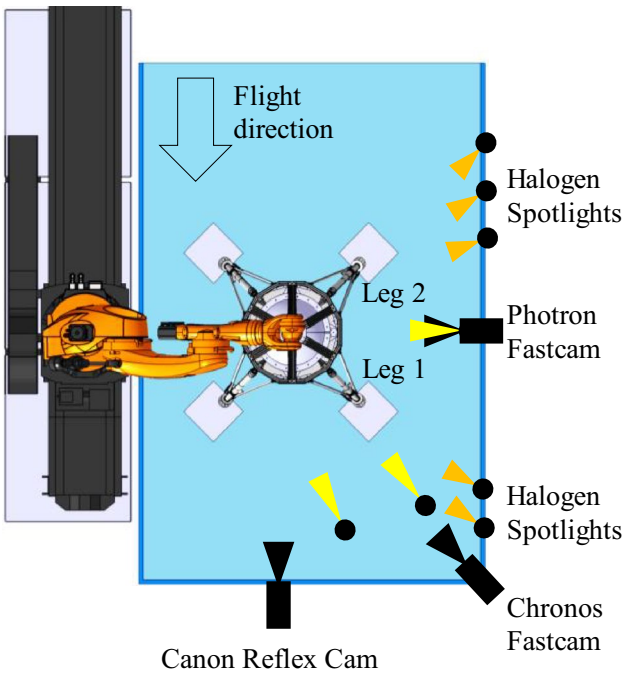

Fig. 6 Spotlight and camera positions

velocity is achieved by the free fall until ground contact. For this campaign the landing zone is equipped with concrete plates, placed on rubber mats to prevent sliding during touchdown. The concrete plates are chosen to ensure defined touchdown conditions in terms of stiffness and roughness.

A camera system is set up for visual documentation and motion tracking, as shown in Fig. 6. Two high-speed cameras are used. High-speed camera 1 (HS1) makes close up videos of the tank during touchdown, where special attention is needed. The HS2 camera is placed in a far perspective of the landing. Both high-speed cameras are mounted on the LAMA fence. A HD reflex camera (canon) is positioned in front of the test setup, providing a front view.

2.3 Test programme

All tests are conducted with a 2–2 configuration, at which the TDD has two leading and two trailing legs. This configuration is chosen to ensure a repeatable tilting axis, which is perpendicular to the horizontal landing velocity vector. The total TDD mass is kept constant throughout the test campaign at approx. 500 kg. The test parameters are driven by two rationale. On one hand, it is aimed for high energy input, within the capability levels of the test facility, to generate significant responses from which the sloshing impact can be derived. On the other hand, the test parameters shall be of comparable magnitude of typical landing test parameters to

ensure structural integrity. During all tests the TDD has the vertical landing velocity of 3.5 m/s, which is comparable to typical VTVL vehicle vertical landing velocities [24, 25]. To investigate the fluid impact on the landing behaviour of the TDD and on the structural responses, drop tests with three different fill levels are conducted:

- Fill level 1: 0 l of water
- Fill level 2: 50 l of water
- Fill level 3: 75 l of water

Fill level 1 serves as reference. At fill level 2 the fluid mass corresponds to 10% of the total TDD mass, which corresponds to maximum residual fuel levels upon touchdown for scientific flight experiments. At fill level 3 approx. 40% of the tank are filled, which correlates with the fill level for which the highest sloshing impact is expected [26]. This fill level range corresponds to expected propellant masses for different VTVL vehicle applications during touchdown. This includes residual propellant mass for successful landing, propellant masses present in landing vehicles, which are supposed to take off and return from extra-terrestrial bodies or propellant masses required as ballistic masses for test flight conditions [27].

For each fill level different horizontal landing velocities are tested, as effects that affect the landing stability and landing dynamics only occur at horizontal landing velocities greater than 0 m/s:

- a) $v_H = 0$ m/s
- b) $v_H = 0.5$ m/s
- c) $v_H = 1$ m/s

Tests with $v_H = 0$ m/s serve as reference and are necessary to examine the structural responses at different fill levels and distinguish between structural responses due to the fluid impact and those due to dynamic effects. As the sloshing amplitude and thus the sloshing impact on the landing dynamics of the TDD are expected to grow with increasing horizontal landing velocity, two additional horizontal velocities are tested. For each fill level tests with $v_H = 0.5$ m/s are conducted. For the fill level extrema of 0 l and 75 l additional tests with $v_H = 1$ m/s are conducted. Both values lie within the capabilities of the test facility and are based on previous landing test campaigns and hence are expected not to peril the structural integrity of the TDD but, nonetheless, induce measurable sloshing impacts.

This results in eight different test cases as listed in Table 1. Two test runs are conducted for each test case to prove non-chaotic and repeatable landing behaviour.

3 Test results and observations

3.1 Repeatability

To ensure repeatable landing behaviour, repeatable landing conditions have to be provided. Inertial robot data show that equal force, acceleration and velocity curves for repetitions of the same test case are achieved. This is shown exemplarily for test runs 3c.1 and 3c.2, which are the ones with highest fluid mass and horizontal landing velocity. The robot interface gripper forces in flight direction $F_{R,x}$ and in vertical direction $F_{R,z}$, the robot velocity in flight direction $v_{R,x}$ and acceleration in flight direction $a_{R,x}$ of test runs 3c.1 and 3c.2 are shown in Fig. 7. Time $t = 0.0$ s marks the release moment, when the interface gripper opens. It can be seen that for both test repetitions equal release conditions are achieved. It shall be noted that the $F_{R,x}$ oscillations before release are also found in test cases without fluid and are due to TDD oscillations resulting from the start up accelerations and not due to sloshing liquid.

Although, the overall test parameters can be kept constant throughout one test case, slight dispersions during the robot release can occur due to friction at the robot interface gripper. The impact of these dispersion is neglectable, as will be shown in the following. Analysis of video data shows constant fluid conditions at touchdown for all test cases. Exemplarily for test run 3c.1 the fluid conditions just before and after touchdown are shown in Fig. 8. No significant sloshing

Table 1 Test plan with test parameters

Case	Fill level (l)	Structural mass (kg)	Extra masses (kg)	Total mass (kg)	v_V (m/s)	v_H (m/s)
1a	0	~375	120	~495	3.5	0
1b	0	~375	120	~495	3.5	0.5
1c	0	~375	120	~495	3.5	1
2a	50	~375	70	~495	3.5	0
2b	50	~375	70	~495	3.5	0.5
3a	75	~375	45	~495	3.5	0
3b	75	~375	45	~495	3.5	0.5
3c	75	~375	45	~495	3.5	1

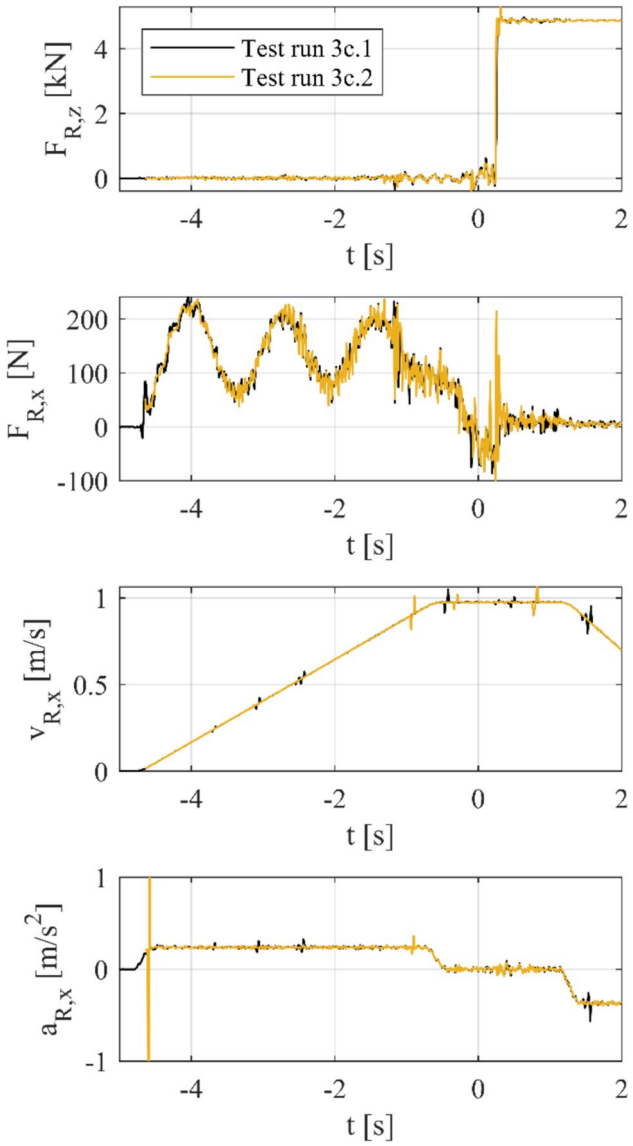

Fig. 7 Robot interface gripper forces in flight direction $F_{R,x}$ and in vertical direction $F_{R,z}$, robot velocity in flight direction $v_{R,x}$ and acceleration in flight direction $a_{R,x}$ for test runs 3c.1 and 3c.2

is detected before touchdown, providing repeatable landing conditions for all tests.

Sensor data of both test repetitions belonging to the same test case are compared with each other to verify repeatable landing behaviour under fluid impact. In the following, sensor data, which are of special significance for the analysis of fluid–vehicle interactions, are presented. This includes tank-lander interface forces, accelerations at the tank bottom plate, tilting motions and footpad forces. Although all test cases are examined, exemplarily only test case 2b is shown, as it is argued that if repeatability can be proven for one test case it can be assumed to be applicable for the others as well.

For the analysis of the fluid impact on the structural responses of the tank-lander interfaces, the tank and the fluid are considered to be one single rigid body. Therefore, instead of analysing each interface force sensor (F_{T1}–F_{T4}) individually, the sum of all tank-lander interface force sensors is considered. The sum of the vertical tank-lander interface forces $F_{TL,v,tot}$ over time for both test runs 2b.1 and 2b.2 of test case 2b is shown in Fig. 9. Time $t = 0.0$ s marks the beginning of the touchdown event, which is defined as the moment of first ground contact of footpad 1. It can be seen that up until approx. 0.15 s after first ground contact amplitude and frequency of the measured forces of both test runs are in high accordance. Frequency deviations are less than 1%. The deviation of the maximum compression forces is less than 1.3% and the deviation of the lower magnitude tensile force maxima is 5.8%. After 0.15 s the curves diverge, indicating a frequency difference in the decay behaviour, which is of minor significance for the fluid–structure interaction analysis and therefore neglectable. As the here compared test repetitions are both conducted with same TDD configurations and test parameters, it is assumed that the deviations are due to slight dispersions in the robot release procedure.

The accelerations in flight direction $a_{T,x}$ (upper plot) and in vertical direction $a_{T,z}$ (bottom plot) at the tank bottom plate over time for both test runs 2b.1 and 2b.2 are shown in Fig. 10. The acceleration curves of both test runs are

Fig. 8 Fluid behaviour before and after touchdown during test run 3c.1

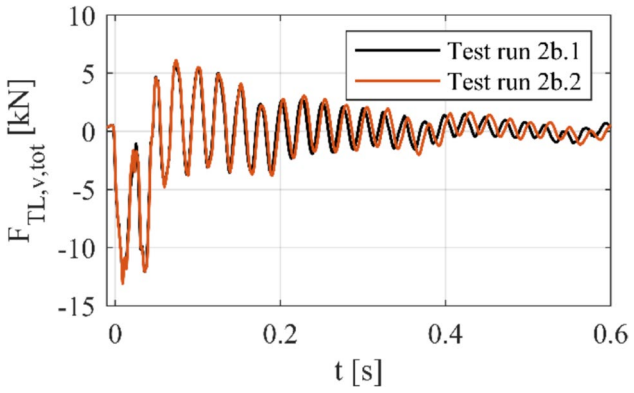

Fig. 9 Sum of vertical tank-lander interface forces $F_{TL,v,tot}$ for test runs 2b.1 and 2b.2

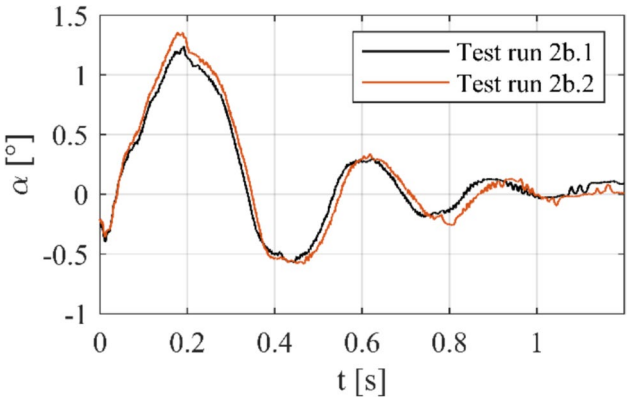

Fig. 11 Tilting angle α for test runs 2b.1 and 2b.2

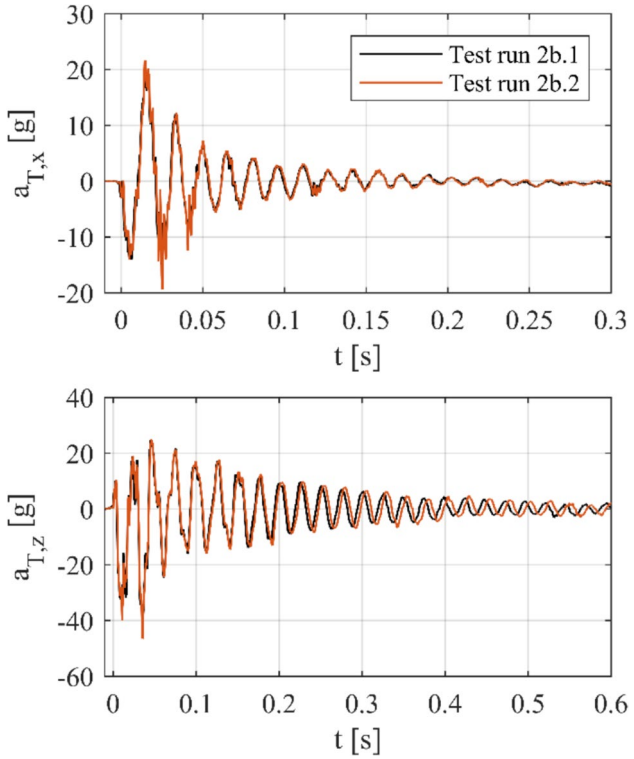

Fig. 10 Acceleration $a_{T,x}$ in flight direction (upper plot) and vertical acceleration $a_{T,z}$ (bottom plot) at tank bottom plate for test runs 2b.1 and 2b.2

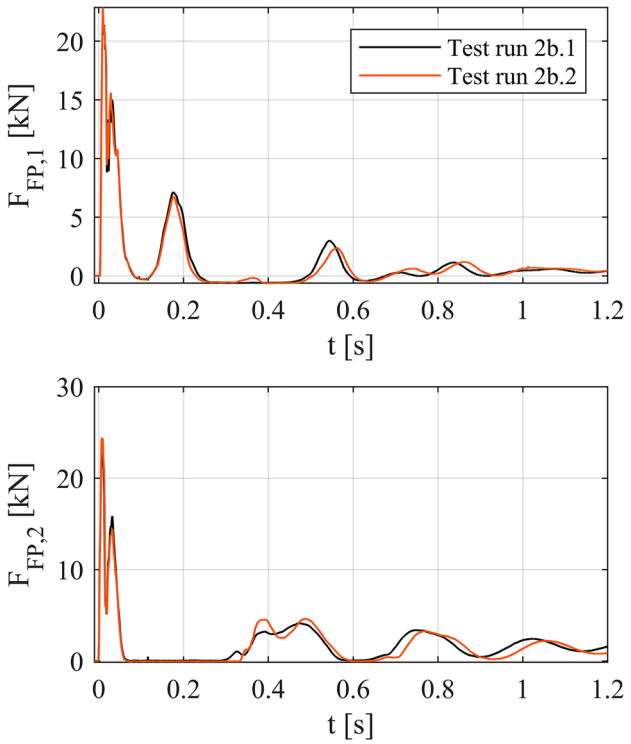

Fig. 12 Footpad forces for test runs 2b.1 and 2b.2

identical for both directions, except for a minor neglectable phase shift in vertical direction, that occurs at approx. 0.2 s, as has been observed in the tank-lander interface force.

The angular displacement, here referred to as the tilting angle α, from the vertically neutral position of the TDD during touchdown for both test runs 2b.1 and 2b.2 is given in Fig. 11. It can be seen that the overall course of both test runs is identical and the test runs correlate in terms of tilting amplitude and frequency. Neglectable differences are only found in the maximum displacements, proving repeatable behaviour in terms of angular displacements.

The footpad forces of footpad 1 $F_{FP,1}$ and footpad 2 $F_{FP,2}$ of test runs 2b.1 and 2b.2 are shown in Fig. 12. Both test runs show the same characteristic curve with only neglectable differences in peak magnitudes. Hence, examination of the here shown data allows the conclusion of repeatable non-chaotic fluid behaviour and thus repeatable fluid–vehicle interactions for constant test conditions.

3.2 Sloshing impact on dynamical landing behaviour

The touchdown event is defined as the time span reaching from the moment of first ground contact until all kinetic energy has ceased. All TDD motions during touchdown can be summarised as dynamical landing behaviour. Within this section, the dynamic landing behaviour of the TDD under the impact of sloshing fluid is investigated with regard to landing stability. For this, the tilting motion of the TDD and the vertical motion in combination with the footpad forces are analysed. Thereby, it is differentiated between

a) the impact of increasing fluid mass on the dynamic behaviour for constant horizontal landing velocities (comparison of test cases 1b, 2b and 3b) and
b) the impact of increasing landing velocities on sloshing-induced effects (comparison of effects observed between 1b and 3b to effects observed between 1c and 3c).

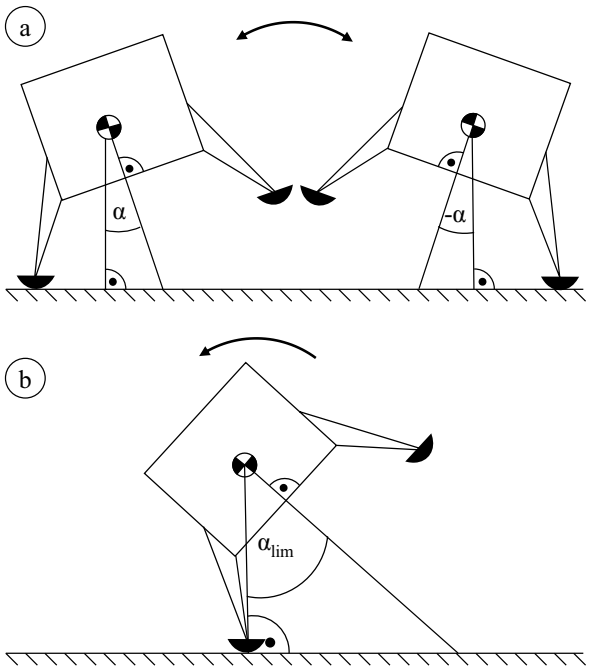

Fig. 13 Tilting motion of a lander with tilting angle α (**a**) and threshold angle α_{lim} (**b**)

3.3 Tilting motion

A stable landing is achieved if the landing vehicle does not tip over during touchdown. Thus, when performing a tilting motion, as shown in Fig. 13 a, the vehicle's tilting angle stays below the stability threshold angle α_{lim} (Fig. 13 b) and decreases with time. The impact of different parameters on the landing stability can therefore be measured by the maximum tilting angle which is achieved during touchdown and the motion decay rate.

The landing sequence of the TDD is shown exemplarily for test case 3b in Fig. 14. The TDD approaches its landing spot with a specific vertical and horizontal velocity (1). Right after touchdown (2), the horizontal landing velocity causes the TDD to tilt in flight direction until a maximum positive tilt angle is reached (3). If the tilt angle was greater than the stability threshold, the TDD would overturn. As in this campaign the stability threshold is not reached, the TDD is tilted back by gravity into its vertically neutral position.

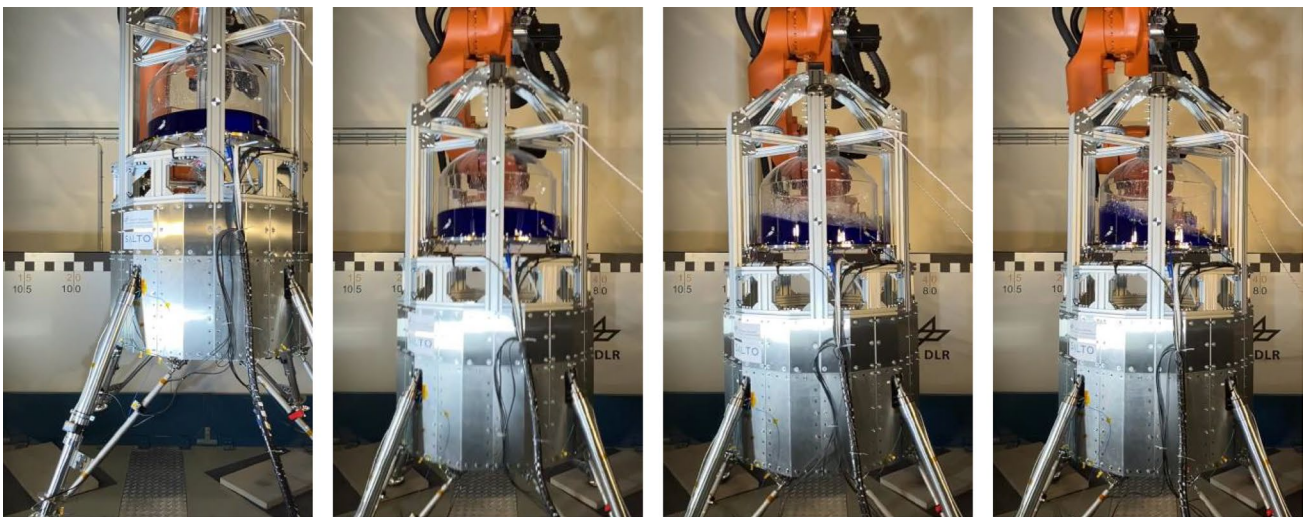

(1) -1.06 s (2) 0 s (3) 0.276 s (4) 0.678 s

Fig. 14 Landing sequence of the TDD

If the kinetic energy has not yet ceased, the TDD will tilt further until a maximum negative tilt angle is reached (4), before tilting into flight direction again. This movement continues until the kinetic energy of the TDD has ceased.

The tilting motion data are retrieved from video analysis using the video analysis software 'Tracker' [28]. The angle is calculated from the vertical and horizontal distances between two marker points on the TDD in a stationary reference coordinate system. The absolute tilt angles α_{abs} for test cases 1b, 2b and 3b over time are given in the upper plot of Fig. 15. In all three test cases the TDD performs a forward and backward tilting motion with decreasing tilt amplitudes, indicating stable landing behaviour, as α_{lim} is not exceeded. In all test cases an end position is reached, where $\alpha_{abs} > 0$, hence the TDD being tilted into flight direction. For test cases 1b and 2b α_{abs} is positive during the entire touchdown event, showing that the TDD does not exceed its neutral position, where $\alpha_{abs} = 0°$, when tilting backwards. Only for test case 3b negative tilt angles are reached. However, as no correlation can be found between the absolute values of α_{abs} and the fluid mass, the negative tilt angles in test case 3b are not considered to be due to the larger fluid mass in this test case.

The bottom plot of Fig. 15 illustrates the normalised tilt angles α_{norm}, which are the angular displacements in relation to the end position. It can be seen that the maximum α_{norm}, which is reached when the TDD is firstly tilted into flight direction, is approx. the same for all test cases. Also, the minimum α_{norm}, which is reached during the first tilt back, is similar in test cases 1b, 2b and 3b. After this, the α_{norm} maxima and the total tilting amplitude decrease with increasing fluid mass, while the α_{norm} minima are lower for higher fluid levels. This implies smaller angular displacements when tilting in flight direction and larger angular displacements when tilting backwards for higher fluid levels. Further, the tilting motion decays faster with larger fluid masses. From this it can be concluded that the fluid causes a dampening effect on the TDD's tilting motion and thus improving landing stability.

To analyse the impact of the landing velocity on the fluid sloshing-induced effects on the tilting motion and thus the landing stability, in Fig. 16 the absolute tilting angle α_{abs} (upper plot) and the normalised tilting angle α_{norm} (lower plot) of test cases 1c and 3c are given. It can be seen that, independently of the fluid mass, an increase in horizontal landing velocity, and thus in kinetic energy,

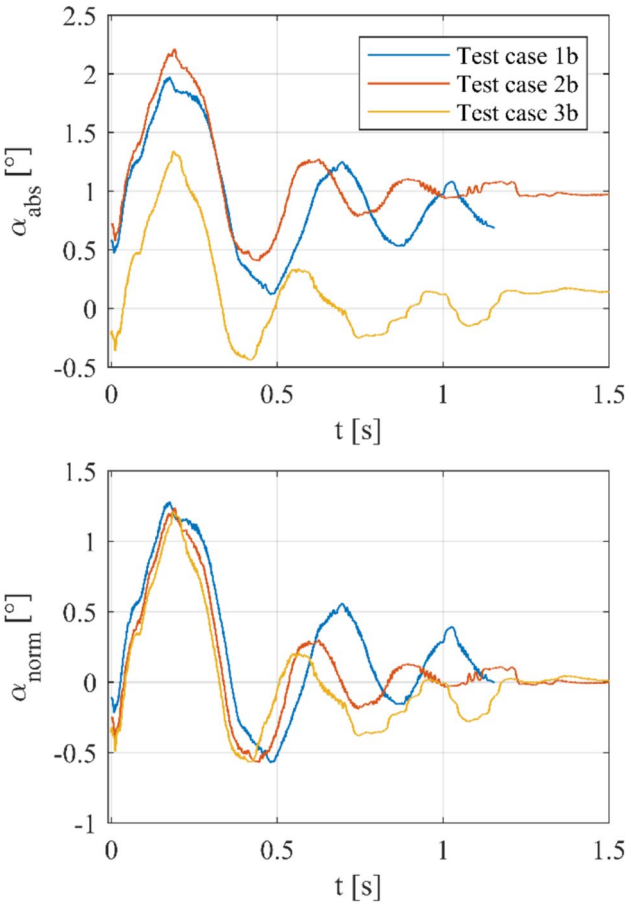

Fig. 15 TDD tilt angle α_{abs} and normalised TDD tilt angle α_{norm} for test cases 1b, 2b and 3b

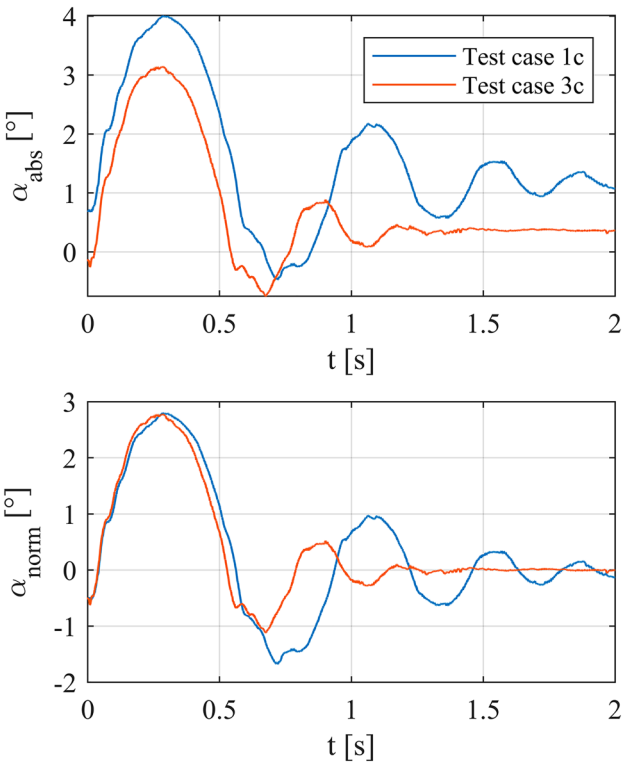

Fig. 16 TDD tilt angle α_{abs} and normalised TDD tilt angle α_{norm} for test cases 1c and 3c

causes larger tilt angles, hence, larger tilt amplitudes and tilt cycle durations. In both test cases 1c and 3c also negative tilt angles are reached.

To determine the impact of the landing velocity on the tilting motion decay rate, the decay rates of test cases 1b, 3b, 1c and 3c are compared and given in Table 2. As for test case 1b not sufficient data are available to identify the absolute time until the tilting motion has ceased, the first three α_{norm} maxima of each test case and the time span between them are used to approximate the decay rates. It can be seen that with higher horizontal landing velocity the tilting motion decay rate of the TDD increases. The fluid impact is determined by comparing the tilting motion decay rates of test cases without fluid (1b and 1c) to those of the test cases with fluid (3b and 3c). A dampening effect of the fluid slosh on the tilting motion is shown, causing up to 1.8 times higher tilting motion decay rates. A non-linear relationship between the fluid damping efficiency and the horizontal landing velocity is detected, as the damping efficiency decreases with increasing horizontal landing velocity. This might be due to several possible reasons, such as sloshing energy dissipation limits or non-linear wave interactions. The investigation of these reasons, however, lies beyond the scope of this study and is to be addressed in the follow-up studies.

Analysis of the fluid motion suggests, the dampening effect could be due to a phase shifted sloshing wave, as shown in Fig. 17. During touchdown part of the kinetic energy is stored in the fluid, causing the fluid to perform a sloshing movement in form of a circulating wave, which counteracts the tilting motion of the TDD.

For all test cases in this campaign, the maximum of the sloshing amplitude on the front tank wall is reached shortly before α_{norm} reaches its local minimum (compare Fig. 18). Thus, the sloshing fluid acts against the TDD movement, causing a returning moment, which has a damping effect on the tilting motion.

3.3.1 Footpad forces

Complementary to the tilting motion analysis, the landing stability is investigated by analysis of the footpad forces. The tilting motion during touchdown is superimposed by a vertical motion, due to elastic resilience through which the footpads lose ground contact. This causes a changing and uneven load distribution in the vehicle's landing legs, which might degrade landing stability. Analysis of the tilting angle, the vertical lander position and the footpad forces of leg 1 and 2 reveals direct correlations between these quantities (compare Fig. 19), which are presented in the following. In a first step, the general courses of the footpad forces and their correlations with the TDD motions are given. In a second step, the fluid impact on these quantities is investigated. As reference quantity for the vertical TDD position the total vertical displacement $s_{v,tot}$ is introduced, which describes the vertical position of an arbitrary marker on the TDD in relation to its final position. This quantity includes the vertical displacement due to the tilting motion and due to elastic rebound jumps.

$F_{FP,1}$ and $F_{FP,2}$, α_{norm} and $s_{v,tot}$ are shown exemplarily for test case 1b in Fig. 19. Both footpad forces show a characteristic double compressive force peak (1,2) shortly after first ground contact. Thereby, the first peak (1) correlates with the first tilting angle minimum (a), which is established right after ground contact before the TDD is tilted into flight direction. The second peak correlates with the minimum total vertical displacement $s_{v,tot}$ (I), which corresponds to elastic deformations after first ground contact. As the TDD is tilted into flight direction and as $s_{v,tot}$ increases, both footpad forces decrease below 0 N (3), indicating a loss of ground contact due to a rebound jump. The front leg, leg 1, regains ground contact and $F_{FP,1}$ begins to increase again as $s_{v,tot}$ reaches a local maximum (II). This results in another compressive force peak (4) when $s_{v,tot}$ reaches a local minimum (III) and the TDD reaches its maximum positive tilting angle (b). When the TDD is tilted backwards and at the same time $s_{v,tot}$ reaches

Table 2 Tilting motion decay rates as calculated for test cases 1b, 3b, 1c and 3c

Maxima considered	Test Case 1b	Test Case 3b	Fluid damping efficiency
$\alpha_{norm,max,1} \rightarrow \alpha_{norm,max,2}$	−1.4°/s	−2.57°/s	1.8
$\alpha_{norm,max,2} \rightarrow \alpha_{norm,max,3}$	−0.48°/s	−0.623°/s	1.3
Maxima considered	Test Case 1c	Test Case 3c	Fluid damping efficiency
$\alpha_{norm,max,1} \rightarrow \alpha_{norm,max,2}$	−2.35°/s	−3.87°/s	1.6
$\alpha_{norm,max,2} \rightarrow \alpha_{norm,max,3}$	−1.36°/s	−1.3°/s	0.96

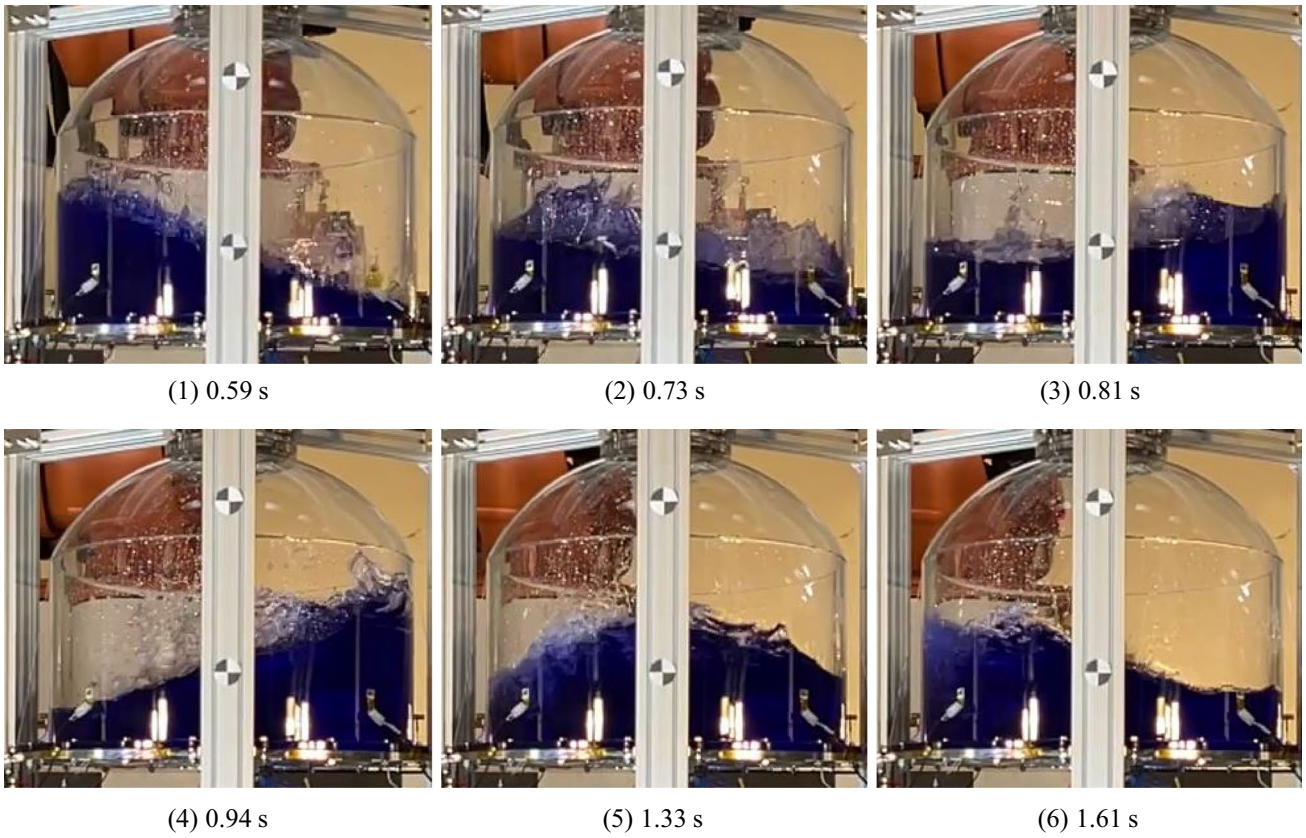

Fig. 17 Circulating sloshing wave

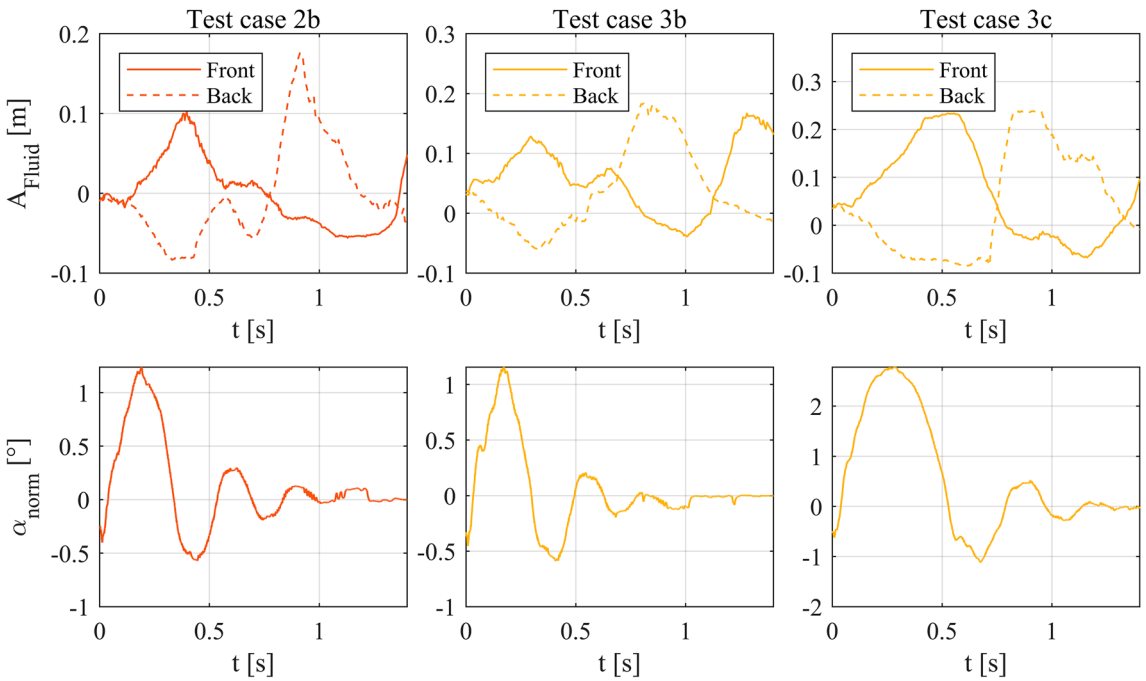

Fig. 18 Fluid amplitude A_{Fluid} at tank wall front and back (top) and normalised tilting angle α_{norm} (bottom) for test cases 2b, 3b and 3c

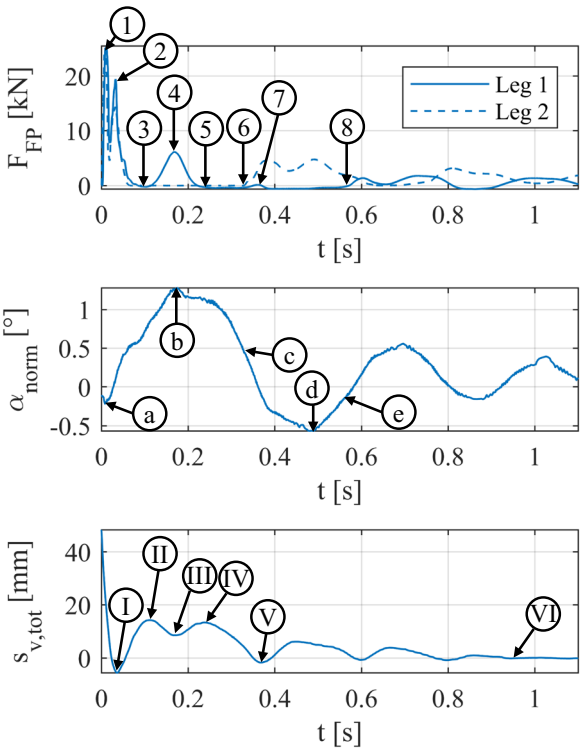

Fig. 19 Footpad forces F_{FP1} and $F_{FP,2}$, normalised tilting angle α_{norm} and total vertical displacement $s_{v,tot}$ for test case 1b

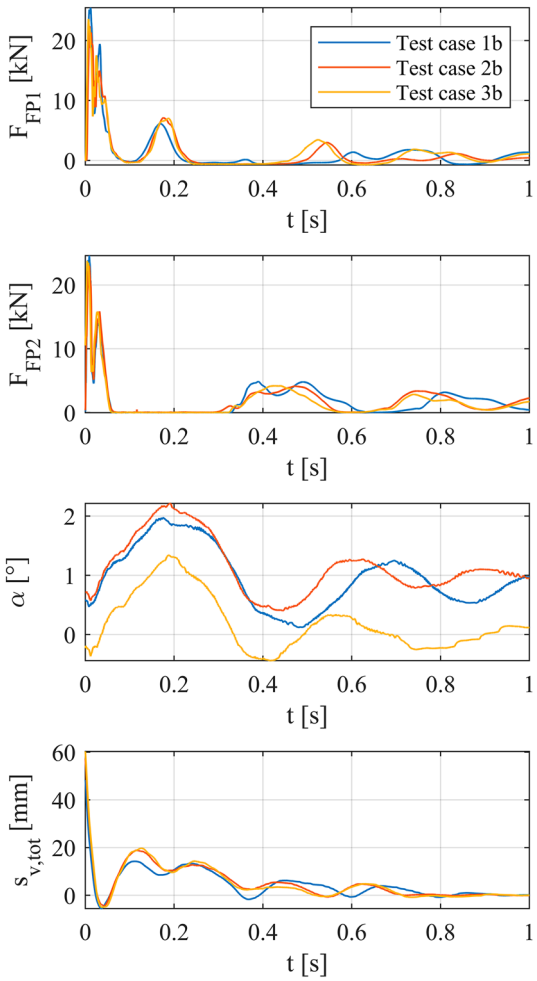

Fig. 20 $F_{FP,1}$ and $F_{FP,2}$, α_{abs} and $s_{v,tot}$ for test cases 1b, 2b and 3b

another local maximum (IV), leg 1 becomes force free again (5), indicating another rebound jump. This is ended as α_{norm} falls below a certain value (c) and the footpads of leg 2 regain ground contact and $F_{FP,2}$ increases (6). During the backwards tilt leg 1 stays force free, except for a short force increase (7), when the TDD falls below its final vertical position, $s_{v,tot}$ reaching another local minimum (V). As the TDD passes its α_{norm} minimum (d), reaching its maximum negative tilting angle, and tilts forwards again. When the tilting angle α_{norm} passes a certain value (e), $F_{FP,1}$ increases again. With decaying $s_{v,tot}$, both footpad forces fluctuate around approx. the same value, alternately falling below 0 N only when the tilting angle maxima are reached. The fluctuation continues beyond the TDD reaching its final vertical position (VI).

To investigate the fluid impact on the footpad forces and thus landing stability, test cases 1b, 2b and 3b are compared. In Fig. 20 the footpad forces of legs 1 and 2 are given for test cases 1b, 2b and 3b. The overall course of both footpad forces is similar in all three test cases. The magnitude of the double force peaks is slightly higher for test case 1b. With rising $s_{v,tot,}$ both footpads lose ground contact, indicating a rebound jump, which is terminated after $s_{v,tot}$ reaches its maximum and the $F_{FP,1}$ increases again. It is noted that with increasing fluid mass, the $s_{v,tot}$ maxima increase and are reached later, correlating with a later $F_{FP,1}$ increase. This indicates a higher and longer first rebound jump for increasing fluid masses.

However, the second rebound jump, which is detected when footpad 1 becomes compression force free again, becomes shorter with increasing fluid mass. This is due to a later second loss of ground contact at footpad 1, corresponding to the later reached local $s_{v,tot}$ minima, and an earlier compression force increase at footpad 2, for increasing fluid mass. Further, permanent ground contact is reached earlier by both footpads for larger fluid masses. This again correlates with the final vertical TDD position being reached earlier in test cases 2b and 3b.

In summary, apart from the longer and higher first rebound jumps, which were found in test cases 2b and 3b, analysis of the footpad forces suggests a stabilising fluid effect on the landing behaviour. This supports the results obtained from the tilting motion analysis.

To investigate the impact of the horizontal landing velocity on the before observed fluid-induced effects, the TDD motions and their impact on the footpad forces in test

cases 1c and 3c are analysed. $F_{FP,1}$ and $F_{FP,2}$, α_{abs} and $s_{v,tot}$ for test cases 1c and 3c are shown in Fig. 21. While in test case 3c a rebound jump is found between 0.2 and 0.4 s, in test case 1c the footpad forces do not both decrease to below 0 N at the same time. Although a vertical motion is performed, the footpads only become compression force free when the tilting angle α_{abs} exceeds a certain threshold value, which depends on the vertical position. The compression force free time spans at both footpads are distinctively shorter in test case 3c, correlating with the higher frequency of the tilting motion. Further, do both footpads reach permanent ground contact earlier in test case 3c, proving a fluid-induced stabilising effect. Although not all fluid effects found in test cases 1b, 2b and 3b could be reproduced at higher landing velocities, the overall fluid-induced stabilisation becomes more pronounced comparing the footpad forces of test cases 1c and 3c.

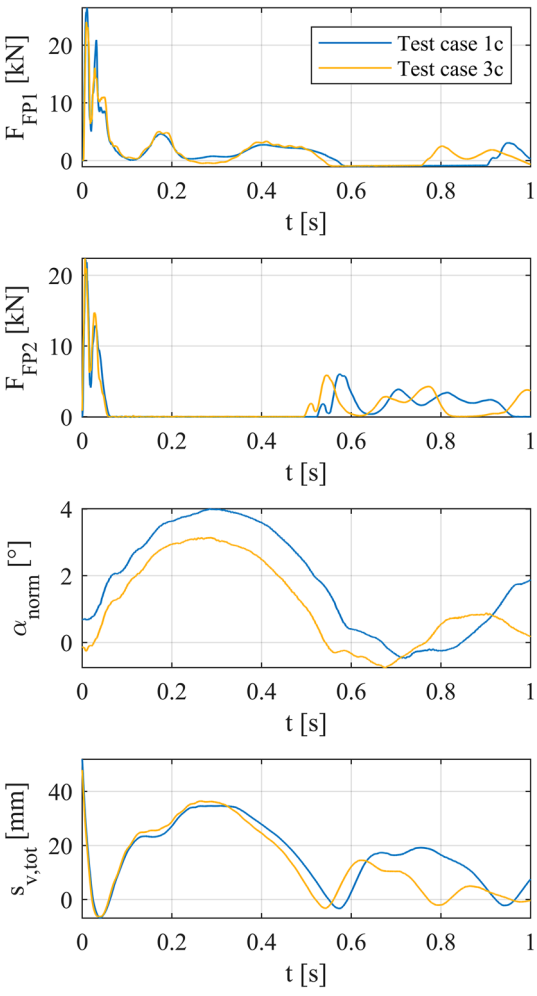

Fig. 21 $F_{FP,1}$ and $F_{FP,2}$ and total vertical TDD displacement $s_{v,tot}$ for test cases 1c and 3c

3.4 Fluid–tank interaction

In the following, the fluid–tank interaction is investigated. For this, the tank–lander interface forces and the structural responses of the tank bottom plate to the touchdown acceleration shocks are analysed. The tank–lander interface forces are examined in the time domain and in the frequency domain. For the characterisation of the fluid impact on the structural responses of the tank bottom plate shock response spectra and amplitude spectra of the touchdown acceleration shocks are analysed. First, test cases with the same horizontal landing velocity but different fill levels are compared to identify the fluid impact on the structural responses. In a next step the observed effects at different horizontal landing velocities are compared to examine if certain effects are damped or amplified through stronger sloshing.

3.4.1 Tank–lander interface forces

The sum of all vertical tank–lander interface forces $F_{tot,TL,v}$ over time (top plot) and the total vertical displacement $s_{v,tot}$ (bottom plot) are shown exemplarily for test case 1b in Fig. 22. The force response is characterised in the time domain by a compressive force peak at first ground contact and a following decaying low frequency oscillation, which is superimposed by a harmonic of higher frequency. Comparison with the $s_{v,tot}$ shows that the $F_{tot,TL,v}$ peak and low frequency oscillation correlate with the vertical motion of the TDD, although not proportionally. For the harmonic no correlation is found, which is why this is the focus of the following investigation.

$F_{tot,TL,v}$ over time is shown for test cases 1a, 2a and 3a in the top plot of Fig. 23. It can be seen that with higher fluid levels and thus higher tank mass, the magnitude of

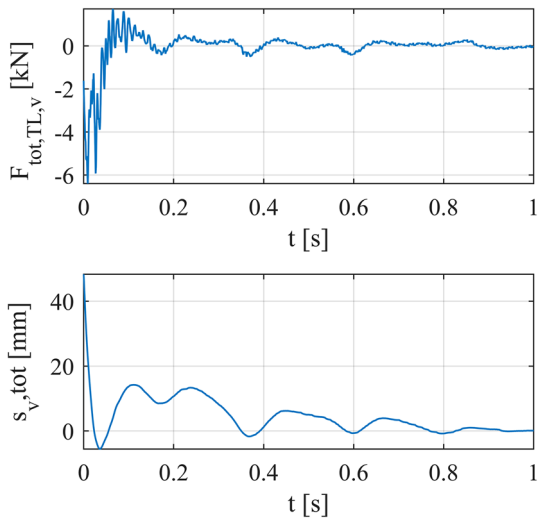

Fig. 22 $F_{tot,TL,v}$ (top) and $s_{v,tot}$ (bottom) for test case 1b

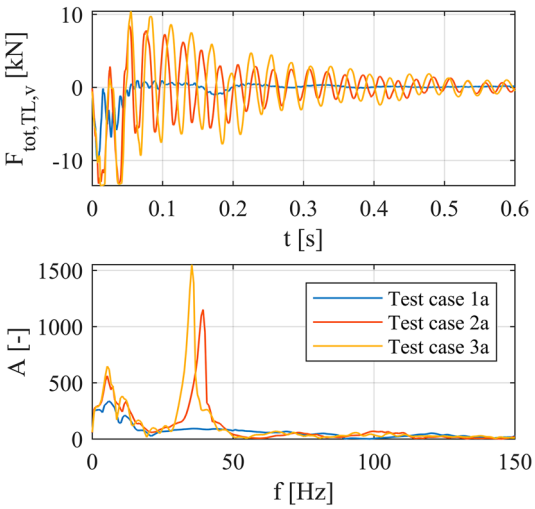

Fig. 23 Amplitude spectrum of total tank–lander interface forces for test cases 1a, 2a and 3a

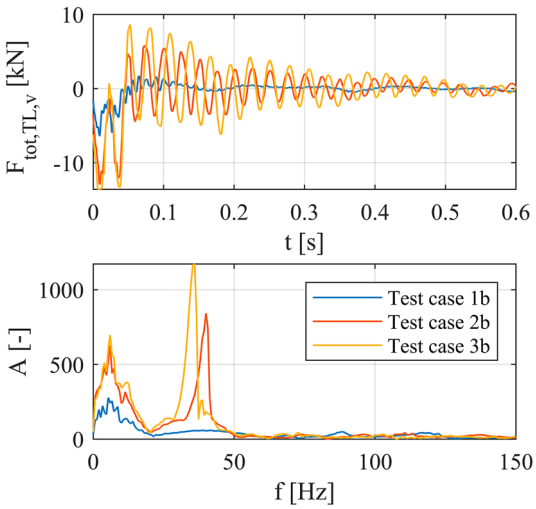

Fig. 24 Total tank–lander interface forces of test cases 1b, 2b and 3b and the corresponding amplitude spectra

the compressive force peak increases. As the gradient is the same in all three test cases, the force peak is reached later with increasing fluid mass. Also, the amplitude of the harmonic increases with increasing fluid level and tank mass. For further investigation of the oscillation an amplitude spectrum of the total vertical tank force is analysed and shown in the bottom plot of Fig. 23. The amplitude spectrum specifies the frequency composition of the force signal. Both the low frequency oscillation and the harmonic are clearly recognisable in the spectrum. For all three test cases the oscillation has a frequency of approximately 5.5 Hz. With increasing fluid level, the fraction of this frequency in the overall signal increases. The harmonic is found at 40 Hz for test case 2a and at 35 Hz for test case 3a, respectively. For test case 1a the frequency is not clearly visible in the spectrum but can be approximated to 88 Hz from data in the time domain, showing a decreasing frequency of the harmonic for increasing fluid mass. As for the low frequency oscillation, the fractions of the harmonic frequencies in the overall signals increase with higher fluid levels.

For test cases 1b, 2b and 3b with $v_H = 0.5$ m/s, $F_{tot,TL,v}$ over time and the corresponding amplitude spectra are given in Fig. 24. For higher fluid levels higher $F_{tot,TL,v}$ peaks are detected in the time domain. In the frequency domain the low frequency oscillation is found at approximately 5–6 Hz, with increasing signal fraction for increasing fluid mass. The harmonic is found at 88 Hz for test case 1b, at 40 Hz for test case 2b and at 35 Hz for test case 3b, again with increasing signal fraction for higher fluid masses.

For the test cases 1c and 3c with $v_H = 1$ m/s, the total tank-lander interface forces (top plot) and the corresponding amplitude spectra (bottom plot) are given in Fig. 25. At 5–6 Hz the low frequency oscillations are found in the amplitude spectra, with increasing signal fraction for increasing fluid mass. At 35 Hz the frequency of the harmonic of test case 3c is found.

Comparing the structural responses at different horizontal landing velocities, shows that the horizontal landing velocity, and thus, the sloshing amplitude has no impact on the observed structural responses. For all tested horizontal landing velocities, the fluid caused a frequency decrease of the harmonic, to the exact same frequency, only dependent on the fluid mass, thus, independently of the horizontal landing velocity. Amplitude and signal fraction of the harmonic are raised with increasing fluid mass.

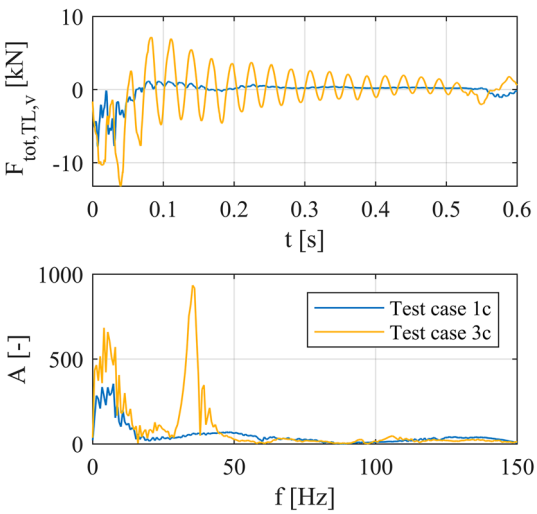

Fig. 25 Total tank–lander interface forces of test cases 1c and 3c and the corresponding amplitude spectra

3.4.2 Structural responses of tank bottom plate

In Fig. 26 a comparison of the amplitude spectra of the vertical tank bottom plate acceleration $Acc_{TBP,v}$ of all test cases is given. These show similarities to the amplitude spectra of the total tank-lander interface forces. For all test cases a peak at a frequency of approx. 6 Hz is found, which is coherent with the frequency of the low frequency oscillation of $F_{tot,TL,v}$ and hence correlates with the vertical TDD motion.

For test cases 1a and 1b, the amplitude spectra of the $Acc_{TBP,v}$ show another peak at approx. 89 Hz, which corresponds to the frequency of the harmonic of $F_{tot,TL,v}$ for these test cases. Under the impact of fluid in test cases 2a, 2b, 3a, 3b and 3c these peaks are shifted to 36 and 40 Hz, respectively. For test cases 1a and 1b additional frequency components, of approximately the same fraction as the 6 Hz and 89 Hz components, are found at 69 Hz and 121 Hz in the corresponding $Acc_{TBP,v}$ amplitude spectra. In test cases with fluid these frequency components cannot be detected.

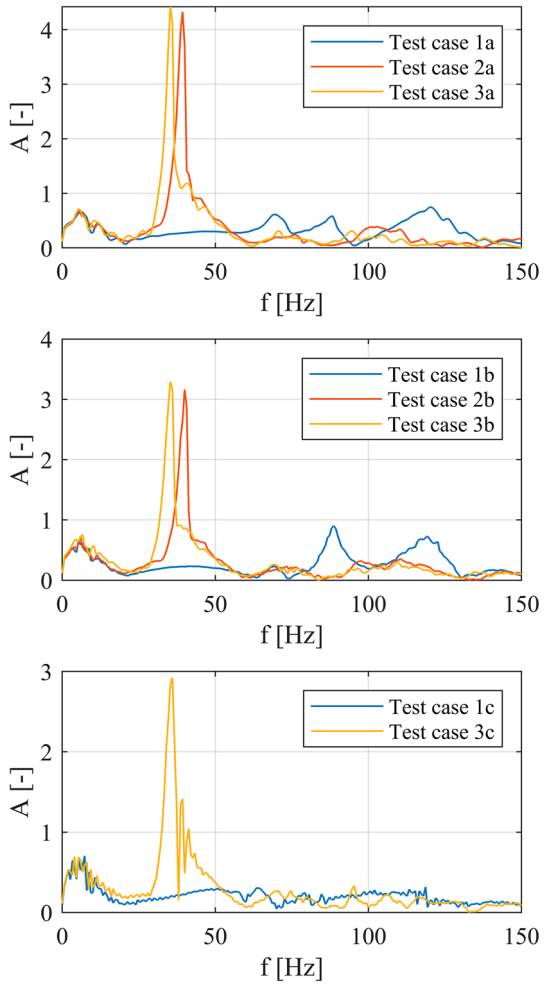

Fig. 26 Amplitude spectra of tank bottom plate accelerations in vertical direction for all test cases

For further investigation of the fluid impact on the structural responses of the tank bottom plate, shock response spectra of $Acc_{TBP,v}$ are analysed. In Fig. 27 the logarithmic shock response spectra of the acceleration shocks at the tank bottom plate for test cases 1a, 2a and 3a are given. These show that, in comparison to an empty tank, the presence of fluid in the tank causes an amplification at frequencies up to approx. 60 Hz, with the highest excitations at approx. 42 Hz. With higher fluid masses the amplification maximum decreases to 40 Hz. For frequencies higher than approx. 60 Hz, the fluid has a dampening effect, which intensifies with increasing fluid mass. This could be due to the fluid acting as a rigid body at low frequencies, interacting with the lowest eigen frequencies of the tank bottom plate. At higher frequencies the fluid does not act as a rigid continuum anymore and high frequency oscillations of the tank bottom plate dissipate inside the fluid. Analysis and comparison of fluid and structure wave modes are, however, beyond the scope of this study and remain to be investigated in the follow-up studies.

In Fig. 28 the shock response spectra of $Acc_{TBP,v}$ for test cases 1b, 2b and 3b are shown. For these test cases with

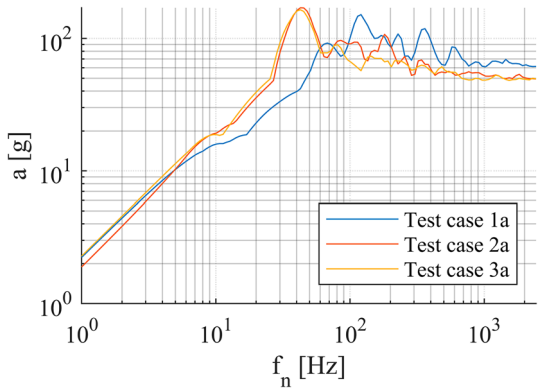

Fig. 27 Shock response spectrum to acceleration shock in vertical direction at tank bottom plate for test cases 1a, 2a and 3a

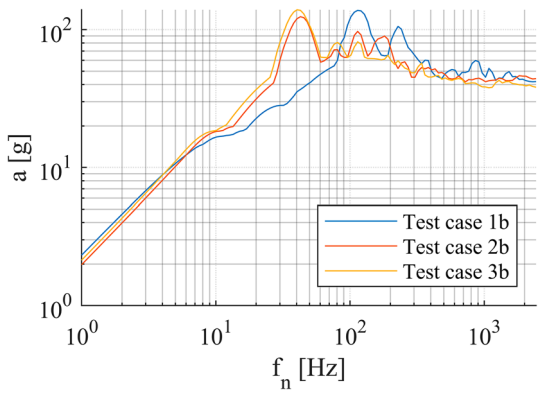

Fig. 28 Shock response spectra to acceleration shocks in vertical direction at tank bottom plate for test cases 1b, 2b and 3b

$v_H = 0.5$ m/s the frequency range, in which the fluid causes an amplified excitation is extended to approx. 80 Hz. The highest amplification is reached at 40 Hz or 42 Hz, respectively. For frequencies higher than approx. 90 Hz the fluid has a dampening effect. The larger the fluid mass, the greater the damping effect.

Comparable to the other test cases, the shock response spectra of $Acc_{TBP,v}$ for test cases 1c and 3c, as shown in Fig. 29, show a fluid related amplifying effect for frequencies up to 100 Hz. The highest amplification is again found at 42 Hz. At frequencies of approx. 100 and 200 Hz a damping effect due to the fluid is detected.

Comparison of the observed fluid effects on the shock responses of the tank bottom plate reveals, depending on the horizontal landing velocity, the fluid has an amplifying effect on the lower frequencies. For a merely vertical landing this amplification ranges to 60 Hz and is extended to approx.100 Hz for horizontal landing velocities of 1 m/s. The highest amplification is unaffected by the horizontal landing velocity and, depending on the fill level, is found at approx. 40 and 42 Hz, respectively. On higher frequencies the fluid has a dampening effect, this transition point shifting from 60 Hz at $v_H = 0$ m/s to 100 Hz for $v_H = 1$ m/s.

4 Summary and conclusions

With the renewed rise in interest in reusable space vehicles a variety of use cases sets new landing requirements for vertically landing spacecraft, which include to carry non-neglectable masses of liquid propellant during touchdown. The open surface in partly filled tanks allows the fluid to slosh when being excited. This causes dynamical and structural interactions between the fluid and the spacecraft or its tank, respectively, affecting the spacecraft's stability and load cases, especially during high impact events, such as touchdown. Therefore, it is indispensable to investigate the fluid–vehicle interactions during touchdown to account for them in the design phase and guarantee for a stable and safe landing. Current studies offer only simplified two-dimensional models to investigate the fluid sloshing impact on the landing behaviour of vertically landing vehicles. Structural fluid–tank interactions during touchdown are not addressed. To contribute to the related research, the presented study experimentally investigated the fluid–vehicle interactions during touchdown of a functional touchdown demonstrator, containing a partly filled tank.

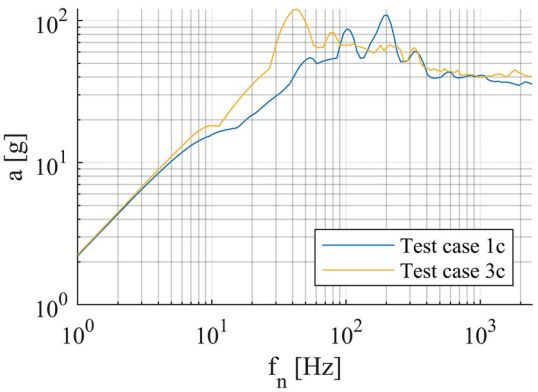

Fig. 29 Shock response spectra to acceleration shocks in vertical direction at tank bottom plate for test cases 1c and 3c

The main findings of this campaign with the here examined parameter combinations can be concluded as follows:

1. To prove repeatable landing behaviour, sensor data of tests with the same landing parameters are compared. For all sensor data of interest for this study, which includes accelerations and forces at the tank, attitude data of the vehicle and impact forces at the footpads, high congruence among tests belonging to the same test case are found. Hence, it is shown that the fluid impact on the landing behaviour is non-chaotic and only dependent on the landing conditions. Based on this finding, data of different test cases can be compared to identify the fluid impact on the landing stability and on the structural responses of the tank.
2. A stable landing is achieved if the landing vehicle does not turn over at ground contact and its motions decay with time. The fluid impact on the landing stability can therefore be identified by analysing the vehicle's motions, which are composed of a tilting motion and a vertical motion due to elastic rebound. Analysis of the tilting angle of the TDD during touchdown shows a decaying tilting motion in all test cases. It is found that with increasing fluid mass the TDD's tilting motion decay rate is increased. Hence, the fluid has a dampening effect on the TDD's tilting motion, which is assumed to be due to a phase shifted circulating wave that counteracts the TDD's motion. At higher landing velocities higher decay rates are reached. However, the fluid tilting damping efficiency decreases at higher landing velocities.
3. The tilting motion of the TDD is superimposed by rebound jumps due to elastic resilience, during which the footpads lose ground contact. This leads to an uneven load distribution and thereby affects the stability budget of the vehicle. Thus, supplementary to the tilting motion, footpad forces and the vertical motion are analysed. The results of these analyses support the ones found through the tilting motion analysis. It is found that the fluid has a stabilising effect on the landing behaviour of the TDD.
4. The investigation of the fluid–structure interaction at the tank is divided into analysis of the vertical tank-to-

vehicle interface forces and the structural responses of the tank bottom plate to the acceleration shocks during touchdown. Correlations between the total vertical tank-lander interface force and the vertical motion are found. The fluid impact on the force response is characterised by shifting the high frequency fractions of the force response to lower frequencies. This corresponds to the findings from the shock response analysis of the tank bottom plate. This reveals that with increasing fluid mass the higher the excitation of lower frequencies through the acceleration shocks at the tank bottom plate during touchdown.

The findings of this study provide a first insight on the fluid–vehicle interactions and their impact on landing dynamics and structural responses depending on varying landing conditions. The obtained results are coherent with those from Roithmayr and Pei, who used a rigid body modelling approach and showed that for certain vehicle configurations and touchdown parameters sloshing could have a stabilising effect on the landing behaviour. Although, it has to be noted, that their work focuses on lunar applications, with landings under lunar gravity. As only one test object was used for this study, the results only apply for a specific set of vehicle parameters. It remains open how the fluid impact changes with varying vehicle and tank configurations. Based on the findings from Roithmayr and Pei it is expected that with increasing H_{COG}/d_F ratio, or at higher landing velocities, the stability boundary is crossed and the fluid slosh has a rather destabilising impact. As their results are based on rigid body assumptions, the influence of flexible vehicle bodies and varying parameters, such as leg elasticity or a variable H_{COG}/d_F ratio on the landing behaviour under fluid impact remain for further investigation. Additionally, only one tank design has been used for this study. Different tank sizes and forms are expected to cause different fluid behaviours which may result in different fluid-induced effects, thus, different landing behaviours or structural responses. The impact of different tank configurations on the fluid–vehicle interaction must be addressed in the follow-up studies.

First indications of structural responses to fluid impact were given by this work. However, the observed phenomena could not be fully explained yet. The reasons for the nonlinear tilting motion damping efficiency of the fluid as well as how mode couplings between fluid and structure affect the structural responses remain unanswered. Also, how different tank configurations affect the structural responses must be answered within the scope of future works.

Many of the here listed open questions can be answered by numerical multibody parameter studies. Based on the test data obtained from this study, a flexible simulation model can be set up and validated and used for numerical parameter studies. This poses a time- and cost-efficient way to investigate the fluid impact for different vehicle parameters, varying tank configurations and fluids with different viscosities to determine stability boundaries, structural responses and interface forces for different touchdown scenarios.

Acknowledgements The authors thank Mr. Silvio Schröder for operating the landing test facility and his support during the test campaign.

Author contribution C.K. wrote the main manuscript text and conducted the test campaign L.W. provided test objectives and supervision All authors are responsible for data analysis and reviewed the manuscript.

Funding Open Access funding enabled and organized by Projekt DEAL. This study was funded by the European Union. Views and opinions expressed are, however, those of the author(s) only and do not necessarily reflect those of the European Union or European Health and Digital Executive Agency. Neither the European Union nor the granting authority can be held responsible for them.

Data availability The authors declare that the data supporting the findings of this study are available within the paper. Data sets generated during the current study are available from the corresponding author on reasonable request.

Declarations

Conflict of interest The authors declare no competing interests.

References

1. *The European Space Agency - Enabeling and Support - THEMIS.* https://www.esa.int/Enabling_Support/Space_Transportation/Themis. Accessed 04.08.2024
2. Iacopino, L.: *SALTO Project.* 21 07 24. https://salto-project.eu/salto-the-new-european-project-ready-to-work-with-reusable-rockets/. Accessed 04.08.2024
3. Ron, H.H., Zupp, G. A.: Apollo lunar module landing dynamics. In: 41st Structures Structural Dynamics, and Materials Conference and Exhibit. American Institute of Aeronautics and Astronautics, Atlanta, GA (2000), https://doi.org/10.2514/6.2000-1678
4. Yu, Q., Wang, T., Li, Z.: Rapid simulation of 3D liquid sloshing in the Lunar Soft-Landing spacecraft. AIAA J. (2019). https://doi.org/10.2514/1.j058160
5. Himeno, T., Watanabe, T.: Sloshing Prediction in the Propellant Tanks of VTVL Rocket Vehicle. In: 41st Joint Propulsion Conference & Exhibit, American Institute of Aeronautics and Astronautics, Tucson (2005). https://doi.org/10.2514/6.2005-3931

6. Himeno, T. et al.: Numerical and experimental investigation on sloshing in rocket tanks with damping devices. In: 43rd Joint Propulsion Conference & Exhibit, American Institute of Aeronautics and Astronautics, Cincinnati, OH (2007). https://doi.org/10.2514/6.2007-5557
7. Lance, A.: Analysis of propellant slosh dynamics and generation of an equivalent mechanical model for the use in preliminary voyager autopilot design studies, technical memorandum No. 33–306, Jet Propulsion Laboratory, California Institute of Technology (1966)
8. Farì, S., Seelbinder, D., Theil, S.: Advanced GNC-oriented modeling and simulation of vertical landing vehicles with fuel slosh dynamics. Acta Astronaut. (2023). https://doi.org/10.1016/j.actaastro.2022.12.035
9. Lunghi, P., Masarati, P., Lavagna, M.: Multibody modeling of sloshing in spacecraft ascent and landing maneuvers. In: Proceedings of the ASME 2016 International Design Engineering Technical Conferences and Computers and Information in Engineering Conference, Vol. 6 Charlotte, NC (2016). https://doi.org/10.1115/DETC2016-59541
10. Pei, J.: Analytical investigation of propellant slosh stability boundary on a space vehicle. J. Spacecr. Rockets (2021). https://doi.org/10.2514/1.A35024
11. Nichkawde, C., Harish, P.M., Ananthkrishnan, N.: Stability analysis of a multibody system model for coupled slosh–vehicle dynamics. J. Sound Vib. (2004). https://doi.org/10.1016/j.jsv.2003.07.009
12. Zhou, R., et al.: Experimental and numerical investigation of liquid slosh behavior using ground-based platforms. J. Spacecr. Rockets (2012). https://doi.org/10.2514/1.A32052
13. Meng, Y., et al.: Predefined-time enhanced antidisturbance attitude control for rigid-liquid coupled launch vehicles. J. Guid. Control. Dyn. (2025). https://doi.org/10.2514/1.G008397
14. Zhou, S., et al.: Numerical simulation of sloshing in the propellant tank of reusable rocket vehicle using meshfree method. Comput. Part. Mech. (2023). https://doi.org/10.1007/s40571-022-00488-4
15. Guo, P., et al.: Liquid propellant sloshing characteristics and suppression in new-generation space vehicle. Aerosp. Syst. (2024). https://doi.org/10.1007/s42401-024-00317-x
16. Zwieten, T. et al.: Nonlinear slosh damping testing and analysis for launch vehicle propellant tanks. In: AIAA Scitech 2020 Forum, https://doi.org/10.2514/6.2020-2050
17. Anii, K. et al.: Dynamics of low-gravity sloshing in spherical tanks during touchdown phases of landers. In: Proceedings of the AIAA Propulsion and Energy Forum (2019). https://doi.org/10.2514/6.2019-4437
18. Furuich, Y. et al.: Evaluation of sloshing effect on a tank during landing phases of spacecrafts in a micro-gravity environment. In: Proceedings of the AIAA Ascend Forum (2022). https://doi.org/10.2514/6.2022-4312
19. Roithmayr, C.M., Pei, J.: Effects of propellant slosh on touchdown stability for landing vehicles. J. Spacecr. Rockets (2024). https://doi.org/10.2514/1.A35791
20. Buchwald, R. et al.: Verification of landing system touchdown dynamics – a status report of a german joint cooperative team on landing technology. In: Proceedings of the 62nd International Astronautical Congress, IAC-11.A3.1.3, Cape Town (2011)
21. Krammer, A., Blecha, L., Lichtenberger, M.: Fin actuation, thrust vector control and landing leg mechanisms design for the RETALT VTVL launcher. CEAS Space J. **14**, 577–591 (2022). https://doi.org/10.1007/s12567-021-00421-0
22. Dumont, E., et al.: Callisto: a demonstrator for reusable launcher key technologies. Trans. JSASS Aerospace Tech. Japan (2021). https://doi.org/10.2322/tastj.19.106
23. https://www.dlr.de/de/forschung-und-transfer/forschungsinfrastruktur/grossforschungsanlagen/lande-und-mobilitaetsanlage. Accessed 04.08.2021
24. Wilken, J., Stappert, S.: Comparative analysis of European vertical landing reusable first stage concepts. CEAS Space J. (2024). https://doi.org/10.1007/s12567-024-00549-9
25. Huang, M.: Control strategy of launch vehicle and lander with adaptive landing gear for sloped landing. Acta Astronaut. (2019). https://doi.org/10.1016/j.actaastro.2019.03.073
26. Benson, D. J., Mason, P. A.: Method for CFD simulation of propellant slosh in a spherical tank. 47th AIAA/ASME/SAE/ASEE Joint Propulsion Conference and Exhibit (2011)
27. Marwege, A. et al.: Retro propulsion assisted landing technologies (RETALT): current status and outlook of the EU funded project on reusable launch vehicles. In: 70th International Astronautical Congress, Washington D.C. (2019)
28. Brown, D., Christian, W., Hansen, R. M.: Tracker video analysis and modeling tool, Downloaded on 15.05.2024 Version 6.1.6, https://physlets.org/tracker/